BIOCHEMISTRY
including biophysical chemistry & molecular biology

Article

pubs.acs.org/biochemistry

Structural and Kinetic Effects on Changes in the CO_2 Binding Pocket of Human Carbonic Anhydrase II

Dayne West,[†] Chae Un Kim,[§] Chingkuang Tu,[‡] Arthur H. Robbins,[†] Sol M. Gruner,[§,∥] David N. Silverman,*[,†,‡] and Robert McKenna*[,†]

[†]Department of Biochemistry and Molecular Biology and [‡]Department of Pharmacology and Therapeutics, University of Florida, Gainesville, Florida 32610, United States

[§]Cornell High Energy Synchrotron Source (CHESS) and [∥]Physics Department, Cornell University, Ithaca, New York 14853, United States

Supporting Information

ABSTRACT: This work examines the effect of perturbing the position of bound CO_2 in the active site of human carbonic anhydrase II (HCA II) on catalysis. Variants of HCA II in which Val143 was replaced with hydrophobic residues Ile, Leu, and Ala were examined. The efficiency of catalysis in the hydration of CO_2 for these variants was characterized by ^{18}O exchange mass spectrometry, and their structures were determined by X-ray crystallography at 1.7−1.5 Å resolution. The most hydrophobic substitutions, V143I and V143L, showed decreases in the level of catalysis, as much as 20-fold, while the replacement by the smaller V143A mutation showed an only moderate 2-fold decrease in activity. Structural data for all three variants show no significant change in the overall position of amino acid side chains in the active site compared with the wild type. However, V143A HCA II showed additional ordered water molecules in the active site compared to the number for the wild type. To further investigate the decrease in the catalytic efficiency of V143I HCA II, an X-ray crystallographic CO_2 entrapment experiment was performed to 0.93 Å resolution. This structure revealed an unexpected shift in the CO_2 substrate toward the zinc-bound solvent, placing it ∼0.3 Å closer than previously observed in the wild type in conjunction with the observed dual occupancy of the product bicarbonate, presumably formed during the acquisition of data. These data suggest that the Ile substitution at position 143 reduced the catalytic efficiency, which is likely due to steric crowding resulting in destabilization of the transition state for conversion of CO_2 into bicarbonate and a decreased product dissociation rate.

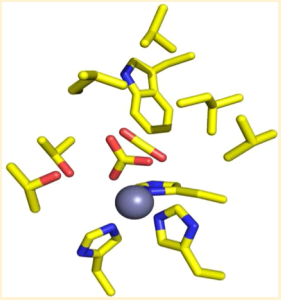

The zinc-containing enzyme human carbonic anhydrase II (HCA II) is the most extensively studied of the carbonic anhydrases and is one of the fastest known enzymes, with a maximal catalytic turnover of 1 μs^{-1}.[1−3] HCA II is widely expressed in cells and tissues, contributing to various physiological processes such as acid−base balance, formation of secretory fluids, and respiration.[4,5] The reaction catalyzed by HCA II in a two-stage ping-pong mechanism is the reversible hydration of CO_2 to bicarbonate and a proton. In the hydration direction, the first stage is the conversion of CO_2 into bicarbonate via a nucleophilic attack on CO_2 by the reactive zinc-bound hydroxide (eq 1). The resultant bicarbonate is then displaced from the zinc by a water molecule. To regenerate the zinc-bound hydroxide, the active form of the enzyme, a proton transfer reaction occurs (eq 2) between the zinc-bound water and external buffer (B) via the proton shuttle residue His 64.[1−3]

$$CO_2 + EZnOH^- \rightleftharpoons EZnHCO_3^- \overset{H_2O}{\rightleftharpoons} EZnH_2O + HCO_3^- \quad (1)$$

$$EZnH_2O + B \rightleftharpoons EZnOH^- + BH^+ \quad (2)$$

The zinc is centrally located in the active site, bound in a tetrahedral coordination with three histidines (His94, His96, and His119) and a solvent molecule (Figure 1). The active site is partitioned into hydrophobic and hydrophilic surfaces on either side of the zinc ion. On one side is a surface of nonpolar amino acids, Val121, Va1143, Leu198, Val207, and Trp209, that form the hydrophobic pocket to which CO_2 binds.[6,7] Detailed crystallographic studies have mapped out the active site of HCA II and demonstrated that one of the oxygen atoms of bound CO_2 interacts with the amide of Thr199 while the other is positioned between the zinc and Val121. This arrangement places the carbon of CO_2 2.8 Å from the oxygen atom of the zinc-bound hydroxide, a position well suited for the nucleophilic attack by the lone pair electrons of the zinc-bound hydroxide oxygen[8,9] (Figure 1). A well-ordered water is also located within the hydrophobic pocket, termed deep water, which is displaced upon binding of CO_2 (Figure 1).[3,6,7,10]

On the opposite side of the active site is a region lined with hydrophilic amino acids (Tyr7, Asn62, Asn67, Thr199, and Thr200) primarily responsible for forming the ordered solvent network that is believed to be necessary for mediating the proton transfer step.[1,11] This network includes five water molecules, the zinc-bound water (Zn-W), W1, W2, W3A, and

Received: August 25, 2012
Revised: October 24, 2012
Published: October 25, 2012

   dx.doi.org/10.1021/bi301155z | *Biochemistry* 2012, 51, 9156−9163

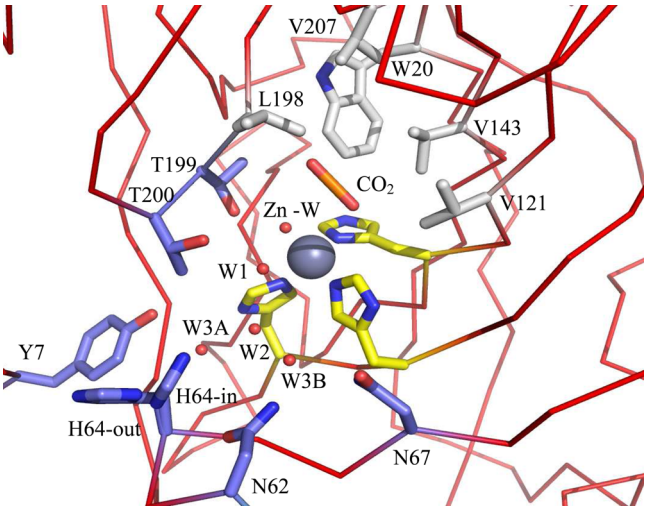

Figure 1. Stick diagram of the active site of HCA II. The substrate CO_2 (orange), active site solvent (red spheres), hydrophobic pocket (light gray), hydrophilic region (blue), and three histidines (yellow) stabilizing the zinc (dark gray). PDB entry 2ILI.[10] Amino acids are as labeled. This figure was generated with PyMol.[32]

W3B, which are stabilized by hydrogen bonds with each other, as well as with hydrophilic side chains (Figure 1). Such a network allows for movement of protons between the zinc-bound solvent and His64 for the transfer of a proton to solution[10] (Figure 1).

Although the binding of CO_2 in the active site of HCA II has been examined by X-ray crystallography,[6,7] the relevance to the catalysis of its position in the enzyme−substrate complex is not well understood. Little is known about the relationship between catalytic efficiency and substrate orientation, a relationship that is difficult to elucidate experimentally. The work presented here focuses on catalysis by variants of Val143 of HCA II and uses X-ray crystallography to elucidate the binding of CO_2 and bicarbonate in the active site of V143I HCA II. There is no significant effect on the structure of ordered waters in the active site cavity in V143I HCA II, and there are only small effects on rate constants for proton transfer. However, the extent of catalysis by V143I HCA II decreased ∼20-fold compared with that of the wild type. The larger side chain of Ile143 in V143I presumably decreases the size of the active site cavity, which results in the CO_2 being 0.3 Å closer to the zinc. This implies a perturbed, crowded transition state that may impede the formation of developing charge on product bicarbonate by the increased hydrophobicity of Ile143. These structural and kinetic studies elucidate the significance of Val143 and the CO_2 binding site in maximizing catalysis.

MATERIALS AND METHODS

Expression and Purification of Mutants. The position 143 HCA II variants were made by site-directed mutagenesis using an expression vector with an HCA II coding region. Single-point mutations were made using the QuikChange II and QuikChange Lightning kits from Agilent. Verification of mutations was accomplished by DNA sequencing of the entire HCA II coding region, followed by simulated translation using *ExPASY* translate. The expression of mutants involved transformation of the mutated plasmid into *Escherichia coli* BL21(DE3)pLysS cells, a cell line specific for protein expression and one that does not express natural CA under our experimental conditions. The cells were transformed and expressed at 37 °C in LB and enriched 2×YT medium, followed by induction with 1 mM isopropyl thiogalactoside when the bacterial growth reached an OD_{600} between 0.6 and

Table 1. Data Processing and Refinement Statistics for the Structures of the HCA II Variants[a]

	V143A	V143I	V143L	V143I (CO_2 bound)
PDB entry	3U3A	3U45	3U47	3U7C
space group	$P2_1$	$P2_1$	$P2_1$	$P2_1$
cell dimensions *a*, *b*, *c* (Å)	42.3, 41.6, 72.3	42.2, 41.3, 72.1	42.3, 41.6, 72.3	42.3, 41.5, 72.1
β (deg)	104.4	104.2	104.5	104.2
resolution (Å)	20−1.7 (1.76−1.70)[f]	20−1.55 (1.61−1.55)	20−1.60 (1.66−1.60)	20−0.93 (0.95−0.93)
R_{sym}[b] (%)	3.7 (9.4)	4.8 (8.8)	4.4 (9.1)	8.2 (44.7)
$I/\sigma(I)$	28.1 (12.8)	28.1 (4.9)	35.9 (5.8)	22.3 (2.4)
completeness (%)	96.7 (98.1)	90.0 (85.4)	90.7 (96.9)	97.2 (85.9)
average redundancy	3.3 (3.2)	4.6 (4.6)	3.2 (3.1)	5.9 (3.2)
no. of unique reflections	26105	31566	29306	157750
R_{cryst}[c], R_{free}[d] (%)	16.0, 19.1	16.2, 19.3	17.9, 21.1	10.6, 13.1
no. of atoms				
protein[e]	2090	2120	2062	2237
water	287	248	288	546
B factor (Å^2)				
protein (main, side)	13.2, 17.4	13.7, 17.1	13.3, 16.6	8.4, 11.3
water	24.8	24.3	25.1	31.9
rmsd for bonds (Å), angles (deg)	0.006, 1.092	0.006, 1.127	0.006, 1.034	0.014, 1.031
Ramachandran plot (%)				
favored	96.9	97.4	96.5	87.1
allowed	3.1	2.6	3.1	12.9
outliers	0.0	0.0	0.4	0.0

[a]Values in parentheses are for the highest-resolution shell. [b]$R_{sym} = (\sum|I - \langle I\rangle|/\sum\langle I\rangle) \times 100$. [c]$R_{cryst} = (\sum||F_o| - |F_c||/\sum|F_o|) \times 100$. [d]$R_{free}$ is calculated the same as R_{cryst}, except with 5% of the data omitted from refinement. [e]The number of atoms varies because of the observed duel conformations of side chains. [f]Indicates statistics in the last resolution bin.

dx.doi.org/10.1021/bi301155z | *Biochemistry* 2012, 51, 9156−9163

1.2, and the addition of 1 mM zinc sulfate to provide a source of zinc for the proper folding and functioning of the enzyme. Cells were harvested 4 h after induction, spun down, and stored in a −80 °C freezer overnight. The cell pellets were lysed, and HCA II was purified via affinity chromatography using *p*-(aminomethyl)benzenesulfonamide.[12] Following purification, the enzyme concentration was determined by titration with the tight-binding inhibitor ethoxzolamide measuring catalyzed ^{18}O exchange.

Crystallization. Crystals of HCA II variants were obtained using the hanging drop vapor diffusion method.[13] The drops were prepared by mixing 5 μL of protein [~10 mg/mL dissolved in 50 mM Tris-HCl (pH 8.0)] with 5 μL of the precipitant solution [containing 50 mM Tris-HCl (pH 8, 8.5, and 9) and 1.3−1.4 M sodium citrate] against 1 mL of the precipitant solution. The drops were allowed to equilibrate at room temperature. The crystal trays were then stored and allowed to sit undisturbed for 1 week.[13] A crystal of each HCA II variant was cryoprotected by being quickly immersed in a 30% glycerol cryoprotectant solution and flash-cooled by being exposed to a gaseous stream of nitrogen at 100 K.

CO_2 Binding. The CO_2 entrapment experiment for a V143I HCA II crystal was achieved by cryo-cooling (~100 K/min) at a pressure of 15 atm of CO_2 as described by Domsic et al.[6] A crystal was soaked in a cryo-solution containing 20% glycerol in a precipitant solution, then coated with mineral oil, and loaded into a high-pressure tube. In the pressure tube, the crystal was pressurized with CO_2 gas at 15 atm at room temperature and cryo-cooled with liquid nitrogen without releasing the CO_2 pressure.[14]

Data Collection. X-ray diffraction data for the HCA II variants were obtained using an in-house R-AXIS IV^{++} image plate system with Osmic Varimax HR optics and a Rigaku RU-H3R Cu rotating anode operating at 50 kV and 22 mA. The detector−crystal distance was set to 76 mm. The oscillation steps were 1° with a 5−7 min exposure per image. Indexing, integration, and scaling were performed using HKL2000.[15] All three data sets that were collected had an average completeness of >90% and a linear R_{sym} of <5.0% (Table 1).

Diffraction data for the CO_2-bound V143I HCA II crystal were collected at the Cornell High Energy Synchrotron Source (CHESS) F1 beamline using a wavelength of 0.9179 Å. Data were collected in 1° oscillation steps with a 3 s time step on an ADSC Quantum 270 CCD detector (Area Detector Systems Corp.), with a crystal−detector distance of 100 mm. The detector was offset to cover the high-resolution diffraction. The data collected had an average completeness of 97.2% and a linear R_{sym} of 8.2% (Table 1).

Structure Solution and Model Refinement. All three in-house HCA II variant structures were determined using the programs *phaser* and *phenix.refine* in PHENIX.[16] Before the refinement, random test sets of ~5% were flagged for R_{free} calculations. The method of structure determination was molecular substitution (*phaser*) with wild-type HCA II (PDB entry 2ILI).[10] The wild-type structure, stripped of the zinc and solvent and with amino acid Val143 replaced with Ala, was used as the initial model for phase calculations in *phenix.refine*. Following three cycles in PHENIX, the refined structure was visually inspected using the molecular imaging system Coot for display of model and electron density.[17] The zinc, the amino acid substitution at position 143, and improperly positioned side chains were manually placed in their respective density. This refined model was then submitted for subsequent rounds of refinement and solvent placement. During the final stages of refinement in conjunction with Coot, the models were viewed and solvent with little or no significant $2F_o - F_c$ density was deleted, until the R_{cryst} and R_{free} values had converged (Table 1).

The CO_2 V143I HCA II structure was similarly refined, but with the addition of dual-occupancy refinement of the both bound CO_2 and bicarbonate (Table 1).

Catalysis. The ^{18}O exchange method relies on the depletion of ^{18}O from CO_2 as measured by membrane inlet mass spectrometry using an Extrel EXM-200 mass spectrometer.[18] In the first stage of catalysis, the dehydration of labeled bicarbonate has a probability of labeling the active site with ^{18}O (eq 3). In a following step, protonation of the zinc-bound ^{18}O-labeled hydroxide results in the release of $H_2{}^{18}O$ to the solvent where it is very greatly diluted by $H_2{}^{16}O$ (eq 4).

$$HCOO^{18}O^- + EZnH_2O \overset{-H_2O}{\rightleftharpoons} EZnHCOO^{18}O^- \rightleftarrows COO + EZn^{18}OH^- \quad (3)$$

$$H^+His64{-}EZn^{18}OH^- \rightleftarrows His64{-}EZnH_2{}^{18}O \xrightarrow{H_2O} His64{-}EZnH_2O + H_2{}^{18}O \quad (4)$$

This approach yields two rates: R_1, the rate of CO_2 and HCO_3^- interconversion at chemical equilibrium (eq 3), as shown in eq 5, and R_{H_2O}, the rate of release of water with labeled substrate oxygen from the enzyme (eq 6).

$$R_1/[E] = k_{cat}{}^{exch}[CO_2]/(K_{eff}{}^{CO_2} + [CO_2]) \quad (5)$$

where $k_{cat}{}^{exch}$ is a rate constant for maximal interconversion of CO_2 and bicarbonate and $K_{eff}{}^{CO_2}$ represents a constant for binding of the substrate to the enzyme. The $k_{cat}{}^{exch}/K_{eff}{}^{CO_2}$ ratio is considered equivalent in value to k_{cat}/K_m from steady-state experiments and is a measure of the successful binding and interconversion of the substrate and product.

The second rate, R_{H_2O}, is the component of the ^{18}O exchange that is dependent upon the donation of protons to the ^{18}O-labeled zinc-bound hydroxide. In such a step, His64 is a predominant proton donor (eq 4) and the value of R_{H_2O} can be determined as the rate constant for the transfer of a proton from His64 to the zinc-bound hydroxide according eq 6. Here k_B is the rate constant for the transfer of a proton to the zinc-bound hydroxide, and $(K_a)_{donor}$ and $(K_a)_{ZnH_2O}$ are ionization constants of the proton donor, His64, and zinc-bound water, respectively. The least-squares determination of kinetic constants of eqs 5 and 6 was conducted using Enzfitter (Biosoft).

$$R_{H_2O}/[E] = k_B/\{[1 + (K_a)_{donor}/[H^+]][1+[H^+]/(K_a)_{ZnH_2O}]\} \quad (6)$$

The uncatalyzed and carbonic anhydrase-catalyzed exchanges of ^{18}O between CO_2 and water at chemical equilibrium were measured in the absence of buffer (to prevent interference from the intermolecular proton transfer reaction) at a total substrate concentration (all species of CO_2) of 25 mM and 25 °C.

Stopped-Flow Spectrophotometry. Initial rates of CO_2 hydration were determined by measuring the change in the absorbance of a pH indicator on an Applied Photophysics SX.18MV stopped-flow spectrophotometer using the method of Khalifah.[19] The pH indicator−buffer pair consisted of *m*-cresol purple (pK_a = 8.3; λ = 578 nm) and TAPS. Final buffer

dx.doi.org/10.1021/bi301155z | *Biochemistry* 2012, 51, 9156−9163

concentrations were 25 mM, and the pH was 8.3. CO_2 solutions were prepared by bubbling CO_2 into water at room temperature (25 °C) at varying CO_2 concentrations. The mean initial rates were measured from five to eight reaction traces comprising the initial 10% of the reaction. Uncatalyzed rates were determined similarly and subtracted from the total observed rates. Determinations of the constants k_{cat} and k_{cat}/K_m were conducted using Enzfitter (Biosoft).

RESULTS

Catalysis. Catalysis by V143I, V143L, and V143A HCA II of the exchange of ^{18}O between CO_2 and water was measured by membrane inlet mass spectrometry. The pH profiles for the catalytic constant $k_{cat}^{exch}/K_{eff}^{CO_2}$ (Figure 2) were adequately fit

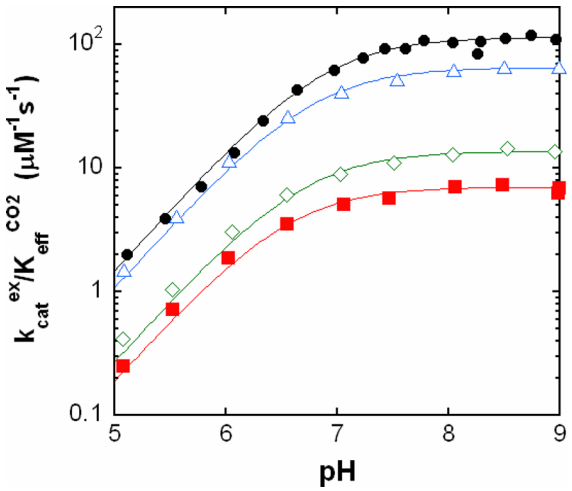

Figure 2. pH profiles of $k_{cat}^{exch}/K_{eff}^{CO_2}$ for the hydration of CO_2 catalyzed by variants of HCA II: wild type (black ●), V143A (blue △), V143I (red ■), and V143L (green ◇). Data were obtained from rates of depletion of ^{18}O from CO_2 measured by membrane inlet mass spectrometry at 25 °C in 25 mM ^{18}O-enriched CO_2/bicarbonate solutions. No buffers were added.

to a single ionization corresponding to the protolysis of the zinc-bound solvent molecule.[1−3] Compared with wild-type HCA II, each of the variants had decreased catalytic efficiency as measured by $k_{cat}^{exch}/K_{eff}^{CO_2}$ (Table 2). Both mutants V143I and V143L showed sizable decreases in the maximal, pH-independent value of $k_{cat}^{exch}/K_{eff}^{CO_2}$ by as much as 17-fold. The variant V143A decreased this efficiency ~2-fold compared with that of the wild type (Table 2). Changes in the rate constant for proton transfer k_B were 2-fold at most (Table 2). The values of the pK_a of the zinc-bound water molecule obtained from the pH profiles of $k_{cat}^{exch}/K_{eff}^{CO_2}$ (Figure 2) and $R_{H_2O}/[E]$ (Figure S1 of the Supporting Information) were not significantly altered compared with those of the wild type (Table 2). However, the values of the pK_a of the imidazole side chain of His64 obtained from pH profiles of $R_{H_2O}/[E]$ were decreased slightly for the mutants (Table 2), an effect seen previously in variants of HCA II in which the orientation of the side chain of His64 was inward.[20]

Table 2. Maximal Values of Rate Constants for the Hydration of CO_2 and Dehydration of Bicarbonate Catalyzed by Variants of HCA II and Related pK_a Values, Obtained by ^{18}O Exchange at 25 °C

	$k_{cat}^{exch}/K_{eff}^{CO_2}$ (μM^{-1} s^{-1})	pK_{ZnH_2O} [a]	k_B (μs^{-1})	pK_{ZnH_2O} [b]	pK_{donor} [b]
wild type[c]	120	6.9	0.8	6.8	7.2
V143A	65 ± 6[d]	6.8	1.4 ± 0.3[d]	6.6	6.6
V143I	7.1 ± 0.2	6.6	0.4 ± 0.1	6.4	6.7
V143L	14 ± 1	6.7	0.7 ± 0.04	6.5	6.5

[a]Obtained from the pH profile of $k_{cat}^{exch}/K_{eff}^{CO_2}$. The standard errors here are ±0.1. [b]Obtained from the pH profiles of R_{H_2O}. The standard errors here are ±0.1 to ±0.2. [c]From ref 11. [d]Standard errors were determined from ^{18}O exchange data as in Figure 2 and Figure S1 of the Supporting Information.

The maximal values of the steady-state catalytic constants for hydration of CO_2 were also measured for these variants by stopped-flow spectrophotometry at pH 8.3. These data show the same trend as the ^{18}O exchange data, with k_{cat}/K_m for V143I and V143L decreased up to 20-fold compared with that of the wild type, while the decrease for V143A is near 3-fold (Table 3). The values of k_{cat}/K_m determined by stopped-flow

Table 3. Steady-State Constants for Catalysis of the Hydration of CO_2 by Variants of HCA II Obtained by Stopped-Flow Spectrophotometry at 25 °C and pH 8.3

	k_{cat}/K_m (μM^{-1} s^{-1})	k_{cat} (μs^{-1})
wild type[a]	120	1.0
V143A	42 ± 1[b]	0.5 ± 0.2[b]
V143I	9.3 ± 0.3	0.7 ± 0.1
V143L	5.5 ± 0.1	1.1 ± 0.3

[a]From ref 31. [b]Standard errors were determined from fits of steady-state data.

methods should in principle be the same as the $k_{cat}^{exch}/K_{eff}^{CO_2}$ values determined in the ^{18}O exchange experiments. Comparison of these values in Tables 2 and 3 shows values that are similar.

Crystal Structures. Using X-ray crystallography, structures of HCA II variants V143A, V143L, and V143I were determined at 1.70, 1.60, and 1.55 Å resolution, respectively. The structures were refined with a final R_{cryst} of <18% (Table 1). The side chains of each of the substituted amino acids at position 143 faced into the active site, in a manner similar to that of the wild type (Figures 1 and 3). Upon comparison of the overall structures of the three variants with wild-type HCA II (PDB entry 2ILI),[10] very minor alterations were noticed on the basis of the structural overlay, which showed an average rmsd of 0.19 Å between Cα atoms in the four superimposed models (Figure 4). For V143A HCA II, the size of the CO_2 binding pocket was increased, and two additional ordered solvent molecules (labeled WA and WB in Figure 3A) were observed. These water molecules are not observed in the wild type or in the other two variants. In addition to these extra solvent molecules in V143A HCA II, and most likely as a consequence of their presence, the solvent molecule termed "deep water" (DW in Figure 3) appears to be 2.7 Å from the oxygen atom of the zinc-bound solvent compared to 2.4 Å in wild-type HCA II. In the V143L variant, the deep water appears to have dual occupancy and is shifted 1.0 Å from the zinc (shown as two red spheres labeled DW in Figure 3B).

Substrate and Product Binding in V143I HCA II. Following the procedures of Domsic et al.,[6] for the entrapment of CO_2 in wild-type HCA II, we examined substrate binding in

dx.doi.org/10.1021/bi301155z | Biochemistry 2012, 51, 9156−9163

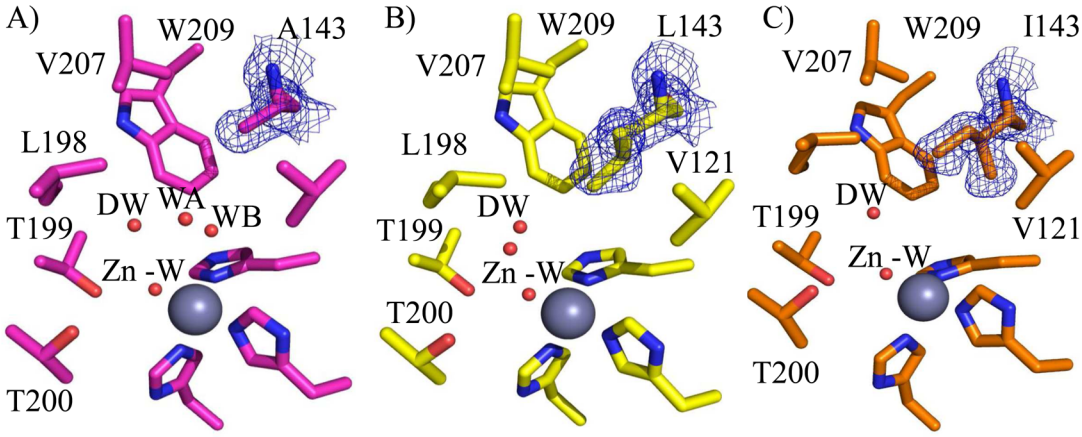

Figure 3. Crystal structure at the active site of (A) V143A (pink), (B) V143L (yellow), and (C) V143I HCA II (orange). Amino acids are as labeled. Shown are the calculated $2F_o - F_c$ electron density map for position 143, contoured at 1.5σ (blue). Solvent molecules are depicted as red spheres and the three histidines coordinating the zinc (dark gray). This figure was generated with PyMol.[32]

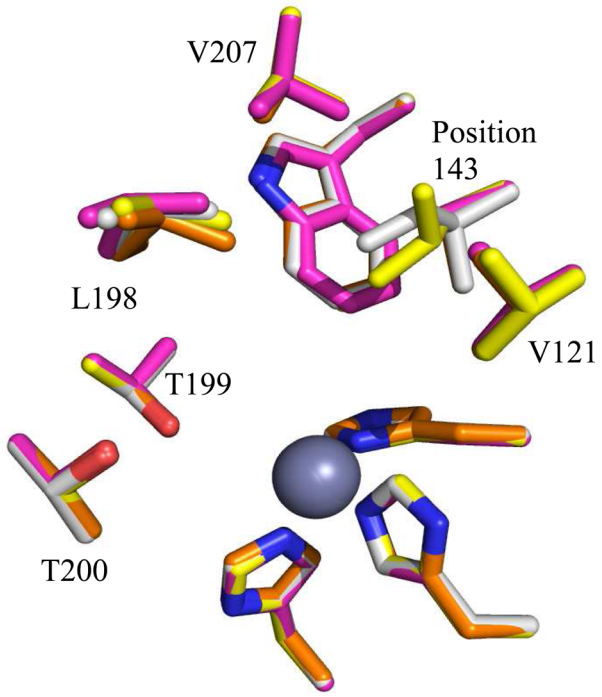

Figure 4. Stick overlay of position 143 HCA II structures. Wild-type (orange), V143A (pink), V143L (yellow), and V143I HCA II (white). Amino acids are as labeled. In addition, the three histidines coordinating the zinc (dark gray) are shown. This figure was generated with PyMol.[32]

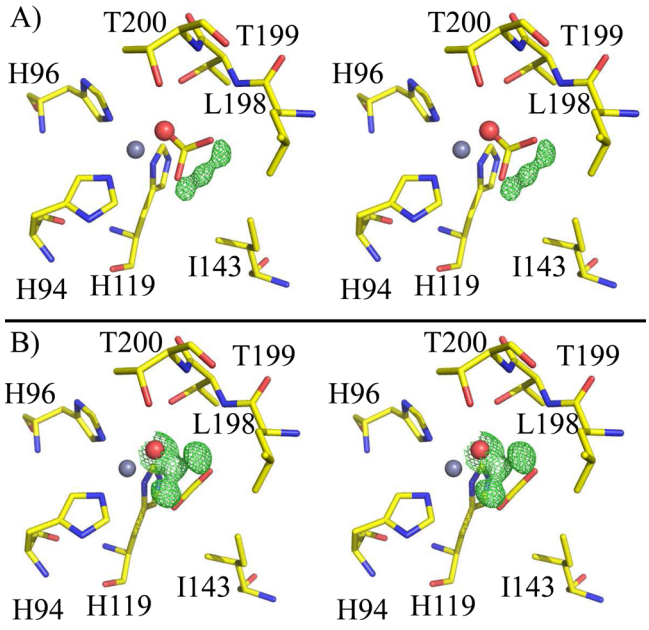

Figure 5. Stick stereo figure of the active site of the V143I HCA II CO_2–bicarbonate complex. Shown are the calculated omit $F_o - F_c$ electron density maps, contoured at 3σ (green), when the (A) CO_2 and (B) bicarbonate were not incorporated into the respective models. The residual electron density in either case indicates the presence of both the substrate and the product. Amino acids are as labeled. This figure was generated with PyMol.[32]

V143I HCA II at a resolution of 0.93 Å. With an rmsd of 0.17 Å between all Cα atoms in the wild type and the V143I variant, superimposition shows good structural agreement. Interestingly, both the substrate CO_2 and product bicarbonate were observed in the active site (Figure 5). This is an interesting observation that contrasts with the wild-type structure in which only CO_2 was observed under these conditions. Hence, careful refinement was performed to determine the occupancy of the CO_2 (0.33), the zinc-bound solvent (0.33), and bicarbonate (0.67). Similar to the wild-type structure of Domsic et al. (PDB entry 3D92), His64 has a dual inward and outward conformation,[21] an unpredictable state in which alterations of HCA II have been introduced. Panels A and B of Figure 5 show the calculated omit $F_o - F_c$ electron density map when the CO_2 or bicarbonate was not incorporated into the respective models. This clearly demonstrates the occupancy of both the substrate and the product (Figure 6).

The CO_2 molecule bound in V143I HCA II is oriented in a side-on conformation similar to that observed by Domsic et al.[6] (Figure 6A). The CO_2 molecule shows similar spatial orientations in both wild-type and V143I HCA II, but with the CO_2 slightly tilted ~10° in the direction of O_2 for the latter. The central carbon atom of CO_2 is noticeably closer to the oxygen atom of the zinc-bound water, now 2.5 Å distant compared to 2.8 Å for the wild type (Figure 7A and Table 4).

The bicarbonate is positioned with O1 and O3 proximal to the CO_2, 1.2 Å from corresponding oxygen atoms of bound

dx.doi.org/10.1021/bi301155z | *Biochemistry* 2012, 51, 9156–9163

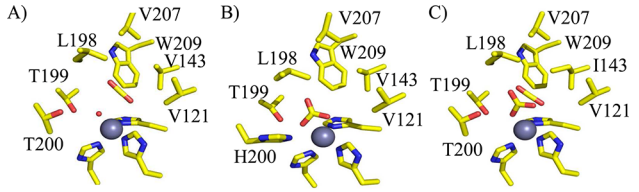

Figure 6. Structure of substrate and/or product bound in HCA II V143I. (A) CO_2 and H_2O molecules (red sphere) in wild type,[6] (B) HCO_3^- in T200H HCA II,[21] and (C) as observed in the crystal structure, with dual occupancy (see Figure 5). Amino acids are as labeled. This figure was generated with PyMol.[32]

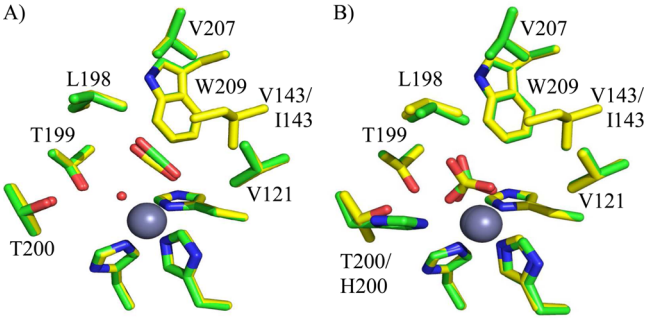

Figure 7. Comparison of HCA II V143I substrate and product binding in HCA II. Structural overlay of (A) CO_2 binding in wild-type (green)[6] and V143I (yellow) HCA II and (B) bicarbonate binding in T200H (green)[21] and V143I (yellow) HCA II. Amino acids are as labeled. This figure was generated with PyMol.[32]

Table 4. Interatomic Distances (in angstroms) for CO_2 in HCA II and Its Variants[a]

atom of CO_2	wild type[b]	wild type[c]	V143I[d]
C	2.8	2.8	2.5
O1	3.0	2.8	2.8
O2	3.1	3.1	2.7

[a]Distances for CO_2 atoms are measured from substrate atoms to the oxygen atom of the zinc-bound solvent. [b]From ref 6. [c]From ref 7. [d]From this work. The uncertainty in these distances is 0.1 Å.

CO_2 (Figure 6B). The other oxygen of the bicarbonate, O2, overlaps with the zinc-bound solvent observed in the CO_2-bound form and coordinates with the zinc, with a distance of 1.9 Å (Figure 6B). Therefore, the three oxygen atoms of bicarbonate "mimic" the spatial oxygen atoms of the CO_2 and the zinc-bound water. The bicarbonate position observed in V143I HCA II overlaps significantly when superimposed with the previously reported coordinates of bicarbonate bound in HCA II T200H (PDB entry 1BIC).[22] The rmsd of all Cα atoms in the V143I and T200H HCA II structures with bicarbonate is 0.33 Å (Figure 7B). The V143I mutant has an 18° rotation of bicarbonate toward the O2 atom compared with that of T200H HCA II. There is also a 0.4 Å separation in carbon atoms between the two superimposed bicarbonate molecules in the T200H and V143I variants.

DISCUSSION

With catalysis nearly diffusion controlled (k_{cat}/K_m of 10^8 M^{-1} s^{-1})[2] and the binding of CO_2 very weak (K_d near 100 mM),[23] HCA II may not have a single well-defined enzyme−substrate complex but an array of CO_2 binding modes that leads to catalysis. An aim of this report is to elucidate the role of the active site configuration in HCA II by perturbing the catalytic binding site of CO_2. Previous work demonstrated that specific replacements of amino acids in the hydrophobic binding pocket of CO_2 are associated with changes in the catalytic rates of HCA II.[23,24] Fierke et al.[24] showed decreases in k_{cat}/K_m for hydration of CO_2 associated with the replacement of Val143 at the CO_2 binding site of HCA II with each of nine amino acids.[24]

The variants of HCA II at residue 143 examined in this report make alterations of the steric volume of the active site cavity while avoiding excessive structural perturbations. The replacements of Val143 in the wild type (side chain volume of 140 Å^3) with Ile (167 Å^3) and Leu (167 Å^3) demonstrate the effects of the decreased steric volume of the cavity and increased hydrophobicity. Val143 was also replaced with Ala (89 Å^3), increasing the volume of the cavity. An overlay of crystal structures of all variants examined in this work showed a superposition of side chain conformations at position 143 with strong side chain overlap in the residues of the active site cavity, indicating that the unaltered residues in the hydrophobic pocket were not significantly affected by the changes in the volume of the active site (Figure 4). Because these replacements do not impinge on the proposed proton transfer pathway,[1] there were rather minor effects on rate constants k_B and k_{cat} that contain contributions of proton transfer between the active site and solvent (Tables 2 and 3).[1,2]

The catalytic efficiency, measured by $k_{cat}^{exch}/K_{eff}^{CO_2}$ (Table 2) and k_{cat}/K_m (Table 3), was decreased up to 20-fold for the replacements of Val143 with larger side chains (Leu and Ile), and to a much lesser extent with a smaller side chain (Ala). These data are in rather close agreement with the stopped-flow results of Fierke et al.[24] It is interesting that even increasing the volume of the active site cavity in V143A HCA II caused a decrease in catalytic activity (Tables 2 and 3).

In the active site, the hydrogen bond between the zinc-bound hydroxide and side chain hydroxyl of Thr199 orients the lone pair electrons of the zinc-bound hydroxyl toward the carbon of CO_2, promoting nucleophilic attack and avoiding an entropic penalty by immobilizing the rotation of the zinc-bound hydroxide about the Zn−O axis.[8−10] In the structure of V143I HCA II, the larger side chain volume of Ile143 compared with that of Val has forced the carbon atom of bound CO_2 closer to the zinc-bound solvent oxygen by a distance of 0.3 Å (Figure 7A and Table 4). This is associated with a 13−17-fold decrease in k_{cat}/K_m and $k_{cat}^{exch}/K_{eff}^{CO_2}$ for hydration when V143I is compared with the wild type (Tables 2 and 3). This sterically crowded active site due to the increased volume of Ile143 is accompanied by the effects of increased hydrophobicity of Ile143 compared with that of Val143 (estimated to be 0.5 kcal/mol based on side chain burial[25]). The overall effect on V143I HCA II is to increase an apparent energy barrier by ∼1.7 kcal/mol for catalysis that in the wild type is near 10 kcal/mol. Such an increase could be an effect of the altered active site on the conversion of CO_2 to bicarbonate, or as mentioned below on the dissociation of the product bicarbonate from the active site. This effect is also the case for V143L, which shows catalytic rates similar to those of V143I HCA II (Tables 2 and 3).

These explanations must be viewed in the context of the decrease, although smaller in magnitude, of catalytic activity when the active site cavity is increased in volume in V143A HCA II. Presumably, here the position of bound CO_2 is more distant from the zinc-bound solvent than in the wild type,

dx.doi.org/10.1021/bi301155z | Biochemistry 2012, 51, 9156−9163

weakening the interaction between the unpaired electrons of the oxygen atom of the zinc-hydroxide and CO_2. Work on the binding of CO_2 to V143A HCA II is in progress.

In the crystal structure of V143I HCA II, we observed the superimposed occupancy of bicarbonate as well as CO_2 (Figures 5 and 6). There are significant changes in the position of bicarbonate upon comparison of binding in V143I HCA II and other reports of bound bicarbonate. It is possible that the shifts are due to the larger side chain of isoleucine in V143I HCA II; however, these changes may be indicative of the influence of the experiment. Previous structures with bicarbonate bound (in T200H HCA II[22] and in T199P/C206S HCA II[26]) diffused bicarbonate into crystals, while our data show the appearance of bicarbonate after the reaction of CO_2 and at the active site. Of course, the various replacements in each variant could promote a change in binding that would explain the observed differences in position. Nevertheless, the bicarbonate molecules in each variant bind directly to the zinc, correlating with the catalytic mechanism of direct nucleophilic attack of zinc-bound hydroxide on CO_2.

Using conditions very similar to those reported here, Domsic et al.[6] did not observe bicarbonate in the crystal structure of wild-type HCA II. However, Sjoblom et al.[7] using repeated X-ray exposure did identify bicarbonate bound in HCA II and suggested that bicarbonate formation was a result of enzyme activation due to radiation-induced events. This implies that increasing the X-ray dose led to enzyme activation, perhaps producing active hydroxyl radicals, which would allow for reaction with CO_2 leading to the formation of bicarbonate, as discussed by Sjoblom et al.[7] Radiation damage is a common issue known to impact macromolecular structures under crystallographic conditions, so this behavior between electrons and water molecules is not unlikely.[27−30] The absorbed dose at which Sjoblom et al. observed bicarbonate was approximately 6×10^6 Gy, and the occupancies were 65% CO_2 and 35% bicarbonate. In the experiment presented here, the data collected for V143I HCA II maintained a constant radiation dose [the estimated radiation dose absorbed at the X-ray beamline used (0.9179 Å wavelength) was 10^6−10^7 Gy], and only one set of data was collected for substrate binding analysis.

The occupancy levels of substrate and product described by Sjoblom et al. are reversed in this study, which found 67% bicarbonate and 33% CO_2 at the active site. The higher occupancy of bicarbonate in this study could indicate a change in the product dissociation rate for V143I HCA II. A decrease in the rate of bicarbonate dissociation could explain the higher occupancy of bicarbonate as well as the decrease in k_{cat}/K_m compared with those of the wild type.

Conclusions. Work reported here demonstrates a role for Val143 in the hydrophobic wall providing a productive binding site for CO_2 in HCA II. Replacement of Val143 with Ile resulted in a decrease in the volume of the active site cavity and a resulting shift in which the position of the carbon in bound CO_2 was 0.3 Å closer to the zinc-bound solvent. This was accompanied by a 17-fold decrease in the level of catalysis compared with that of the wild type. These results are consistent with the binding of CO_2 to the hydrophobic wall including Val143 as being productive in catalysis.[3,24] In fact, Val143 is highly conserved among the carbonic anhydrases in the α class. These data help in the development of a possible structure−function relationship between the position of the substrate in the enzyme−substrate complex and the catalytic efficiency. Observing specific changes in the binding of substrate related to catalytic activity provides insight into the catalysis and may provide pathways to variants of carbonic anhydrase with specifically engineered catalytic activity for industrial and environmental uses.

■ ASSOCIATED CONTENT

Supporting Information

pH profile of the rate constants $R_{H_2O}/[E]$ for HCA II, V143A HCA II, V143L HCA II, and V143I HCA II. This material is available free of charge via the Internet at http://pubs.acs.org.

■ AUTHOR INFORMATION

Corresponding Author

*R.M.: Department of Biochemistry and Molecular Biology, College of Medicine, University of Florida, Box 100245, Gainesville, FL 32610; phone, (352) 392-5696; fax, (352) 392-3422; e-mail, rmckenna@ufl.edu. D.N.S.: Department of Pharmacology, College of Medicine, University of Florida, Box 100267, Gainesville, FL 32610; phone, (352) 392-3556; fax, (352) 392-9696; e-mail, silvrmn@ufl.edu.

Funding

This work was supported by National Institutes of Health (NIH) Grant GM 2515. CHESS is supported by the National Science Foundation and the National Institute of General Medical Sciences (NIGMS) via NSF Grant DMR-0936384, and the MacCHESS resource is supported by NIGMS Grant GM-103485.

Notes

The authors declare no competing financial interest.

■ ACKNOWLEDGMENTS

We thank Dr. Ken Merz for helpful comments.

■ ABBREVIATIONS

HCA, human carbonic anhydrase; V143A HCA II, variant of human carbonic anhydrase with Val143 replaced with Ala; rmsd, root-mean-square distance; 2×YT, 2× yeast extract and tryptone; PDB, Protein Data Bank.

■ REFERENCES

(1) Silverman, D. N., and McKenna, R. (2007) Solvent-Mediated Proton Transfer in Catalysis by Carbonic Anhydrase. *Acc. Chem. Res. 40*, 669−675.

(2) Lindskog, S. (1997) Structure and mechanism of carbonic anhydrase. *Pharmacol. Ther. 74*, 1−20.

(3) Christianson, D. W., and Fierke, C. A. (1996) Carbonic anhydrase: Evolution of the zinc binding site by nature and by design. *Acc. Chem. Res. 29*, 331−339.

(4) Supuran, C. T., Scozzafava, A., and Conway, J. (2004) *Carbonic Anhydrase: Its Inhibitors and Activators*, CRC Press, Boca Raton, FL.

(5) Chegwidden, W. R., Carter, N. D., and Edwards, Y. H. (2000) *The Carbonic Anhydrases: New Horizons*, Birkhauser Verlag, Basel, Switzerland.

(6) Domsic, J. F., Avvaru, B. S., Kim, C. U., Gruner, S. M., Agbandje-McKenna, M., Silverman, D. N., and Mckenna, R. (2008) Entrapment of Carbon Dioxide in the Active Site of Carbonic Anhydrase II. *J. Biol. Chem. 283*, 30766−30771.

(7) Sjoblom, B., Polentarutti, M., and Djinovic-Carugo, K. (2009) Structural study of X-ray induced activation of carbonic anhydrase. *Proc. Natl. Acad. Sci. U.S.A. 106*, 10609−10613.

(8) Merz, K. M. (1991) CO_2 Binding to Human Carbonic Anhydrase-II. *J. Am. Chem. Soc. 113*, 406−411.

(9) Merz, K. M. (1990) Insights into the Function of the Zinc Hydroxide-Thr199-Glu106 Hydrogen-Bonding Network in Carbonic-Anhydrases. *J. Mol. Biol. 214*, 799−802.
(10) Fisher, S. Z., Maupin, C. M., Budayova-Spano, M., Govindasamy, L., Tu, C., Agbandje-McKenna, M., Silverman, D. N., Voth, G. A., and McKenna, R. (2007) Atomic crystal and molecular dynamics simulation structures of human carbonic anhydrase II: Insights into the proton transfer mechanism. *Biochemistry 46*, 2930−2937.
(11) Fisher, S. Z., Tu, C. K., Bhatt, D., Govindasamy, L., Agbandje-McKenna, M., McKenna, R., and Silverman, D. N. (2007) Speeding up proton transfer in a fast enzyme: Kinetic and crystallographic studies on the effect of hydrophobic amino acid substitution in the active site of human carbonic anhydrase II. *Biochemistry 46*, 3803−3813.
(12) Khalifah, R. G., Strader, D. J., Bryant, S. H., and Gibson, S. M. (1977) C-13 Nuclear Magnetic-Resonance Probe of Active-Site Ionizations in Human Carbonic-Anhydrase B. *Biochemistry 16*, 2241−2247.
(13) McPherson, A. (1982) *Preparation and Analysis of Protein Crystals*, Wiley, New York.
(14) Kim, C. U., Kapfer, R., and Gruner, S. M. (2005) High-pressure cooling of protein crystals without cryoprotectants. *Acta Crystallogr. D61*, 881−890.
(15) Otwinowski, Z., and Minor, W. (1997) Processing of X-ray Diffraction Data Collected in Oscillation Mode. *Methods Enzymol. 276*, 307−326.
(16) Adams, P. D., Afonine, P. V., Bunkoczi, G., Chen, V. B., Davis, I. W., Echols, N., Headd, J. J., Hung, L. W., Kapral, G. J., Grosse-Kunstleve, R. W., McCoy, A. J., Moriarty, N. W., Oeffner, R., Read, R. J., Richardson, D. C., Richardson, J. S., Terwilliger, T. C., and Zwart, P. H. (2010) PHENIX: A comprehensive Python-based system for macromolecular structure solution. *Acta Crystallogr. D66*, 213−221.
(17) Emsley, P., and Cowtan, K. (2004) Coot: Model-building tools for molecular graphics. *Acta Crystallogr. D60*, 2126−2132.
(18) Silverman, D. N. (1982) Carbonic anhydrase: Oxygen-18 exchange catalyzed by an enzyme with rate-contributing proton-transfer steps. *Methods Enzymol. 87*, 732−752.
(19) Khalifah, R. G. (1971) Carbon Dioxide Hydration Activity of Carbonic Anhydrase. 1. Stop-Flow Kinetic Studies on Native Human Isoenzyme-B and Isoenzyme-C. *J. Biol. Chem. 246*, 2561−2573.
(20) Mikulski, R. L., and Silverman, D. N. (2010) Proton transfer in catalysis and the role of proton shuttles in carbonic anhydrase. *Biochim. Biophys. Acta 1804*, 422−426.
(21) Nair, S. K., and Christianson, D. W. (1991) Unexpected pH-Dependent Conformation of His-64, the Proton Shuttle of Carbonic Anhydrase-II. *J. Am. Chem. Soc. 113*, 9455−9458.
(22) Xue, Y. F., Vidgren, J., Svensson, L. A., Liljas, A., Jonsson, B. H., and Lindskog, S. (1993) Crystallographic Analysis of Thr-200 → His Human Carbonic-Anhydrase II and Its Complex with the Substrate, HCO_3^-. *Proteins: Struct., Funct., Genet. 15*, 80−87.
(23) Krebs, J. F., Rana, F., Dluhy, R. A., and Fierke, C. A. (1993) Kinetic and Spectroscopic Studies of Hydrophilic Amino-Acid Substitutions in the Hydrophobic Pocket of Human Carbonic Anhydrase-II. *Biochemistry 32*, 4496−4505.
(24) Fierke, C. A., Calderone, T. L., and Krebs, J. F. (1991) Functional Consequences of Engineering the Hydrophobic Pocket of Carbonic Anhydrase-II. *Biochemistry 30*, 11054−11063.
(25) Karplus, P. A. (1997) Hydrophobicity regained. *Protein Sci. 6*, 1302−1307.
(26) Huang, S., Sjoblom, B., Sauer-Eriksson, A. E., and Jonsson, B. H. (2002) Organization of an efficient carbonic anhydrase: Implications for the mechanism based on structure-function studies of a T199P/C206S mutant. *Biochemistry 41*, 7628−7635.
(27) Borek, D., Cymborowski, M., Machius, M., Minor, W., and Otwinowski, Z. (2010) Diffraction data analysis in the presence of radiation damage. *Acta Crystallogr. D66*, 426−436.
(28) Ravelli, R. B. G., and Garman, E. F. (2006) Radiation damage in macromolecular cryocrystallography. *Curr. Opin. Struct. Biol. 16*, 624−629.
(29) Carugo, O., and Carugo, K. D. (2005) When X-rays modify the protein structure: Radiation damage at work. *Trends Biochem. Sci. 30*, 213−219.
(30) Sippel, K. H., Genis, C., Govindasamy, L., Agbandje-McKenna, M., Kiddle, J. J., Tripp, B. C., and McKenna, R. (2010) Synchrotron Radiation Provides a Plausible Explanation for the Generation of a Free Radical Adduct of Thioxolone in Mutant Carbonic Anhydrase II. *J. Phys. Chem. Lett. 1*, 2898−2902.
(31) Steiner, H., Jonsson, B. H., and Lindskog, S. (1975) Catalytic Mechanism of Carbonic-Anhydrase: Hydrogen-Isotope Effects on Kinetic-Parameters of Human C Isoenzyme. *Eur. J. Biochem. 59*, 253−259.
(32) DeLano, W. L. (2002) *The PyMOL Molecular Graphics System*, DeLano Scientific, San Carlos, CA.